Crack Interactions of Non-Coplanar Internal and External Surface Cracks of Hollow Thin Cylinders

Omar Mohammed Al-Moayed ¹, Zainun Achmad ², and Al Emran Ismail ³*

¹ Renewable Energy Research Center, University of Anbar, Ramadi, Iraq ² Department of Mechanical Engineering, Universitas 17 Agustus 1945, Surabaya, Indonesia ³ Faculty of Mechanical and Manufacturing Engineering, Universiti Tun Hussein Onn Malaysia, Batu Pahat, Malaysia Email: omar.m.f@uoanbar.edu.iq (O.M.A-M.); zainun@untag-sby.ac.id (Z.A.); emran@uthm.edu.my (A.E.I.) *Corresponding author

Abstract—The interaction of noncoplanar internal and external surface cracks in hollow thin cylinders plays a critical role in structural integrity assessments, particularly under cyclic and multi-axial loading conditions. The objective of this study is to investigate the behavior of noncoplanar parallel cracks under tension, bending, torsion, and mixed-mode loading, focusing on the distribution of normalized Stress Intensity Factors (SIFs) and the interaction effects along the crack front. ANSYS finite element software is used to model the cracks, and SIFs are extracted along the crack front using the Interaction Integral Method (IIM). Results indicate that external cracks exhibit asymmetric SIF distributions with both amplification and shielding effects, while internal cracks primarily experience shielding. Crack depth (a/t ratio) and separation distance (s/L) significantly influence the interaction magnitude, with deeper cracks showing stronger amplification effects. Under torsional loading, shielding dominates, and interaction effects diminish with increased crack separation. Additionally, the inclination angle affects crack interaction behavior, with external cracks demonstrating greater amplification, making them more critical for structural failure. The findings provide valuable insights into crack growth behavior and fracture mechanics in thin-walled cylinders, aiding in the development of improved damage tolerance design and life extension strategies for critical structural components.

Keywords—crack interaction, non-coplanar surface cracks, hollow thin cylinder, stress intensity factor, ANSYS finite element analysis, fracture mechanics, crack assessment

I. Introduction

Crack propagation and fracture mechanics play a crucial role in the structural integrity of cylindrical components used in aerospace, automotive, and pressure vessel applications. Hollow thin cylinders are particularly susceptible to fatigue-induced cracking due to cyclic loading conditions, making the study of crack behavior essential for ensuring durability and safety [1-5]. The presence of internal and external surface cracks can significantly alter the stress distribution within the material, leading to crack interaction effects that influence the overall failure mechanisms. These interactions, governed by factors such as crack depth, separation distance, inclination angle, and loading conditions, determine whether cracks experience amplification or shielding effects, ultimately affecting their growth rate and propagation direction. While previous studies have extensively analyzed single cracks [6–12], there remains a need for a comprehensive investigation into the interaction of multiple noncoplanar cracks under various loading scenarios [12–32]. This study aims to address this gap by evaluating the Stress Intensity Factors (SIFs) of noncoplanar parallel cracks in thin-walled cylinders under tension, bending, torsion, and mixed-mode loading. The findings will provide valuable insights into crack interaction mechanisms, contributing to the development of improved design modifications and life extension strategies for critical structural components.

II. LITERATURE REVIEW

The Fractal-like Finite Element Method (FFEM) was performed to study the interaction behavior by means of SIFs of multiple penny-shaped cracks located on a solid cylinder subjected to tensile loading [13]. The cracks are oriented symmetrically and parallel to one another on the cylinder. The considered crack numbers are 1, 2, 3, and 7 parallel cracks. The SIFs results revealed that the strength of multiple-cracked structures is higher than that of a single crack under similar conditions. Also, small distances between cracks result in small SIFs, which lead to high structural strength in the case of multiple cracks. In addition, in the case of multiple parallel cracks, SIFs for the inner cracks are less compared to SIFs of a single crack case by 16% to 48%. Besides, the farthest crack, which is the nearest crack to the boundary in case of several cracks holding the highest values of SIFs, is likely to fail first.

The interaction of two parallel surface cracks on a solid cylinder subjected to remote tensile loading was

Manuscript received March 13, 2025; revised March 20, 2025; accepted April 15, 2025; published October 14, 2025.

determined in Ref. [14]. Where SIFs are considered the driving force; therefore, SIFs have been determined along the crack front by Finite Element Method (FEM). Different crack geometries and separation distances were used to cover a wide range, for aspect ratios from 0.2 to 1.2, while the ratio of crack depth to cylinder diameter was between 0.1 and 0.4. Meanwhile, the normalized separation distance between the cracks, c/l, is considered as 0.005, 0.01, 0.02, 0.04, 0.08, 0.16, and 0.32. By considering the interaction factor as the ratio of the SIFs for the case of a double crack to the SIFs of a single crack, three points along the crack front have been selected to check the interaction factor for those points; they are the surface point, the deepest point, and a point between them.

Based on the results of this study, higher SIFs are attained for deeper cracks and vice versa. It is also found that, because of the interaction between the cracks, SIFs decrease due to the increase in cylinder flexibility. The increase in the separation distance between the cracks leads to a diminishing of the interaction.

In Ref. [15], mode I SIFs have been evaluated for single and multiple numbers of axial surface cracks located on a pressurized thick hollow cylinder. The examined configuration is shown in Fig. 1, where the FEM has been utilized to obtain SIFs. In Fig. 1, opposite multiple cracks are used where crack interactions are studied and analyzed. Moreover, this study examined the cylinder with an external to internal diameter ratio of 2, and N number of cracks. Where N = 1, 2, 4, 8, 16, 32 cracks, these cracks vary with aspect ratio from 1 to 4, and relative depth from 0.05 to 0.5. The aim was to correlate the FE results for single and multiple crack cases, which were then used to derive empirical expressions for mode I SIFs at the deepest and surface points on the crack front. Based on the findings, closed-form equations have been introduced to quantify the impacts of crack shape and depth on the SIFs for single and arrays of similar cracks at the inner surface of a thick hollow cylinder.

However, this study did not consider the circumferential crack type, which is common in hollow cylinders. Besides, in terms of crack geometry, this study considered a high crack aspect ratio from 1 to 4, while sharp cracks (cracks with a low aspect ratio) are more risky than transverse cracks. Also, the study did not examine the interaction for high depths of cracks since the range for the relative depth of the cracks was from 0.05 to 0.5 only. The relative depth of the cracks has a significant effect on the SIFs value since deep cracks have SIFs higher than those of cracks less in depth. Thus, this will affect the crack interaction calculation. The only mode I SIFs have been determined, while cylinders in practice may be exposed to different types of loadings, which leads to different modes of failure in the cylinders. Therefore, it is essential to investigate the crack interaction under different types of loading.

To determine the interaction behavior of two coplanar longitudinal cracks positioned in a cylinder, Finite Element Analysis (FEA) and Fracture Mechanics (FM) analyses were conducted [16]. This study considered the stress field close to the crack tip as the main parameter for the crack interaction. Therefore, in FEA, the J-integral as

well as the stress field were evaluated to determine the interaction of the fracture driving force. Based on the results, this study introduced an equivalent crack driving force to perform more realistic assessments for the crack interaction problem, due to the cumulative application of conservative measures, and to prevent unrealistic structural integrity assessments. Nevertheless, this study dealt with two axial coplanar cracks only and did not examine the behavior of circumferential cracks.

The interaction of semi-elliptical cracks located in a pressurized hollow cylinder has been investigated in this study by 3D analysis using FEM [17]. The axial cracks were oriented radially, and this study considered several cracks from 2 to 180. These cracks have different configurations and geometries depending on the utilized crack parameters, that is, a/c from 0.2 to 2, and a/t from 0.05 to 0.6. Based on the findings of this study, the case of two cracks is more critical than other cases with a greater number of cracks, and the least-squares fit is employed to propose two expressions for this case.

In the two cracks case, like all others, when the crack depth increases and its ellipticity decreases, the maximum SIFs grow to a large value, generating a more critical situation. However, this study dealt with axial cracks only, and a single type of loading was examined, which is internal pressure. In terms of the crack geometry, this study did not consider deep cracks (high relative depth of the crack) despite their influence on the crack interaction.

In addition to Ref. [18], where this study examined the interaction effect of internal axial coplanar surface cracks located on the internal surface of a pressurized thick cylinder. FEM is used to perform 3D analysis. A wide variety of crack configurations were used in terms of crack geometrical parameters, where this study considered a/c from 0.2 to 2, a/t from 0.05 to 0.6, and 2 c/d from 0.25 to 0.99 (d, is the separation distance between the cracks). The analysis was presented to determine the impact of the three main factors, the number of cracks, the crack shape (ellipticity), and the depth of the crack, on the interaction factor between nearby cracks. Where mode I SIFs for all the examined cases have been evaluated. The results of this indicated that the number of cracks has an opposite effect on SIFs, where the increase in the number of cracks produces an increase in SIFs.

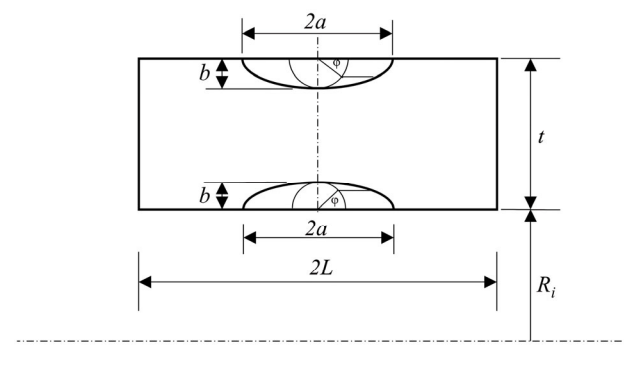


Fig. 1. Pressurized cylinder with internal and external cracks.

In addition, longitudinal crack arrays are more crucial as ellipticity expands. Besides, the depth of the crack for

all the considered cases, as it is, increases, presenting an increment in SIFs. However, this research is dedicated to studying the crack interaction of longitudinal cracks under internal pressure only, where the circumferential crack type is not examined, as well as the other loading types that may produce different modes of failure. Besides, since SIFs are strongly influenced by the depth of the crack, it is vital to examine the crack interaction for cracks with a relative depth of the crack higher than 0.6, which is the maximum considered depth in this research.

The interaction between longitudinal external and internal cracks located in a cylindrical pressure vessel was investigated in Ref. [19]. The hybrid boundary element method is employed to perform numerical analysis to determine the SIFs for a broad range of crack and cylinder geometries. For the cylinder geometry, t/Ri is assumed to be 0.1 and 0.25, while for the crack geometry, b/a ranges from 0.25 to 1, and 2 b/t varies from 0.2 to 0.7, all the dimensions defined in Fig. 1 [20–27].

III. MATERIALS AND METHODS

In this work, a thin-walled cylinder is considered as tabulated in Table I, while Table II reveals crack geometries used and Fig. 2 shows the crack nomenclature used. When the geometries of the cylinder and crack are modeled in the ANSYS finite element program, the only output parameter is the SIF with the unit of MPmm^{0.5}. For the parallel crack configuration, two surface cracks are positioned on the outer and inner surfaces of the hollow cylinder separately. The cracks are named Crack 1 and Crack 2; they are separated by the horizontal separation distance, s, as shown in Figs. 3(a) and 3(b). In this case, the normalized SIFs are presented first for this configuration in terms of the distribution of the normalized SIFs along the crack front, then the interaction factor, Ψ is calculated for three points on the crack front: A, B, and C as shown in Fig. 4.

The second examined crack configuration is the noncoplanar parallel cracks as shown in Fig. 3(b). Where the two cracks were assumed to be inclined by an inclination angle α with respect to the Y-axis. Since two types of cylinders were examined, for each, a different crack geometry was applied; thus, for each type of cylinder, three values of α were used, such as 5°, 10°, and 15°. It is also considered that s was taken as 3 mm, 6 mm, 12 mm, and 24 mm, and then, s was utilized in the normalized form, s/L; thus, s/L was taken to be 0.004, 0.008, 0.016, and 0.032.

The cracks are inserted into the model using the semi-elliptical crack option; this option requires specifying many parameters related to the crack. Two sections must be stated for the crack: the scope and definition, as shown in Fig. 5. In the scope section, geometry selection is required to detect the general location of the crack or the body that contains the crack, which is, in this case, the cylinder. The definition section contains several parameters:

(1) Coordinate system: for each crack, a separate coordinate system was created, which specifies the exact location of the crack on the cylinder in terms

- of external or internal crack. It is also used to quantify the distance between the cracks as well as the inclination angle of each crack.
- (2) S Major and minor radius of the crack, where they represent the half-length, c, and depth, a, of the crack, respectively. Each value is listed in Tables I and II for thick and thin cylinders individually.
- (3) Mesh method, which is selected as Hex Dominant in the present study, as recommended. Moreover, the largest contour radius and crack front divisions must be specified, where for the largest contour radius, three values were used: 0.2 mm, 0.5 mm, and 0.8mm, depending on the a/t ratio, and crack front divisions were selected to be 25.
- (4) Circumferential divisions and mesh contours, for the circumferential divisions selected to be 16, and for mesh contours, selected as 6.

TABLE I. THIN-WALLED CYLINDER AND CRACK GEOMETRIES

Item	Thin cylinder
Internal Diameter, Di	200 mm
Outer Diameter, Do	250 mm
Wall Thickness, t	25 mm
Length, L	750 mm
t/R_i	0.25
t/D _i	0.125 > 0.05 (1/20)

TABLE II. CRACK GEOMETRIES

a/t	t (mm)	a (mm)	a/c	c (mm)
0.2	10	2	0.4	5.0
0.5	10	5	0.4	12.5
0.8	10	8	0.4	20.0
0.2	10	2	0.6	3.33
0.5	10	5	0.6	8.33
0.8	10	8	0.6	13.33
0.2	10	2	0.8	2.5
0.5	10	5	0.8	6.25
0.8	10	8	0.8	10.0
0.2	10	2	1.0	2
0.5	10	5	1.0	5
0.8	10	8	1.0	8
0.2	10	2	1.2	1.67
0.5	10	5	1.2	4.17
0.8	10	8	1.2	6.67

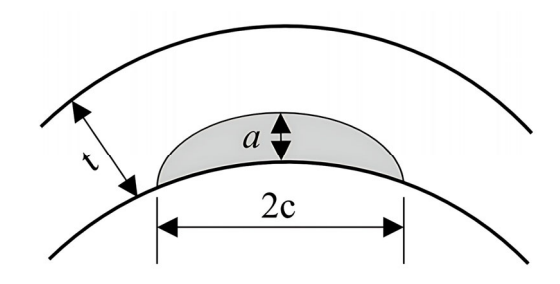


Fig. 2. Crack nomenclatures.

On the other hand, noncoplanar parallels are shown in Fig. 6. Four types of loading conditions were examined for each type of crack configuration: tension, bending, torsion, and mixed-mode loading. In the case of mixed-mode loading, tension, bending, and torsion are combined and applied to the cracked structure. Generally, based on the

literature, the vast majority employed remote constant loading in their research.

In terms of boundary conditions, both ends of the cylinder are fixed so that there is no axial displacement, and the radial displacement is free to move. To prevent the body's rotation, one arbitrary point is fixed in all degrees of freedom.

Therefore, all the above-mentioned loads were applied remotely to the cylinder by using a remote point, since it is commonly used. Moreover, the remote point was linked to one end of the cylinder, where the load was applied through it, while the other end was fixed with zero degree of freedom.

In the present work, since the problem is considered in the Linear Elastic Fracture Mechanics (LEFM) region, the SIFs are assumed as the driving force for the interaction between the cracks where the Interaction Integral Method (IIM) is used to determine the SIF and the SIFs are normalized according to Eq. (1).

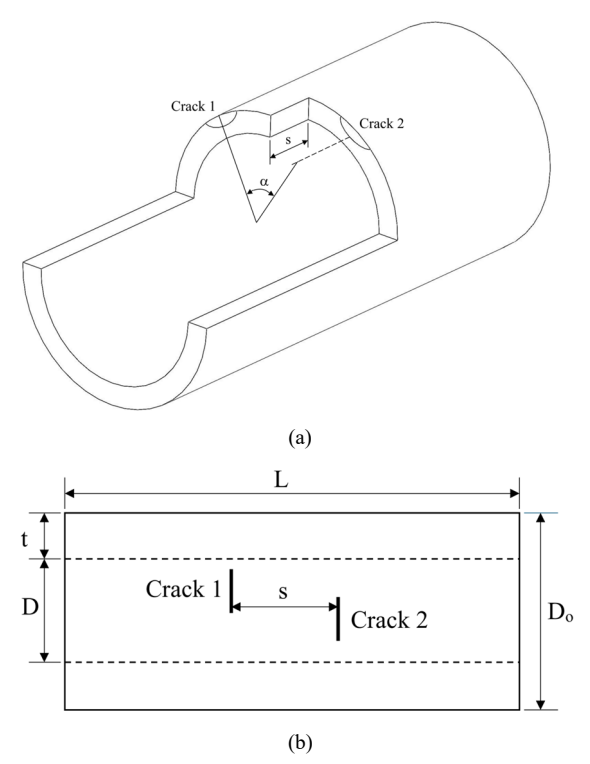


Fig. 3. Noncoplanar parallel crack configuration (a) isometric view, (b)

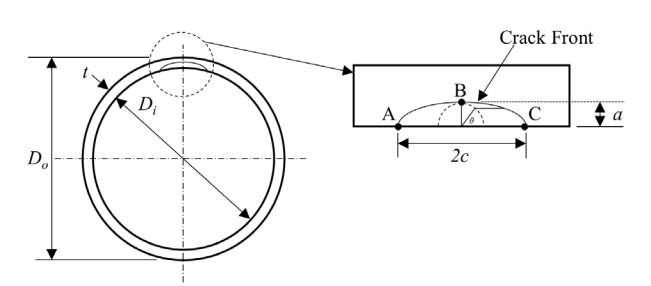


Fig. 4. Noncoplanar parallel crack configuration.

$$F = \frac{K}{\sigma \sqrt{\frac{\pi a}{Q}}} \tag{1}$$

Where F is the normalized SIF, K is a stress intensity factor determined by ANSYS finite element software, Q is the shape factor and σ is a stress produced by tension force, bending moment, torsion moment, and combination of all stresses.

The interaction factor Ψ , defined as the ratio of the SIFs for the case of two cracks to the SIFs of a single crack; therefore, the following expression is used to determine the interaction factor as in Eq. (2).

$$\psi = \frac{F_{\text{two-cracks}}}{F_{\text{single-crack}}} \tag{2}$$

where $F_{two\text{-cracks}}$ represents the normalized SIFs for the case of two cracks for any mode and type of loading, and $F_{single\text{-crack}}$ is the normalized SIFs for the case of a single crack. Moreover, the Ψ for tension loading, for example, is the ratio of the normalized SIFs for the case of two cracks with respect to normalized SIFs for the single crack case in tension loading. This procedure is applicable to the remaining types and modes of loadings.

On the other hand, the crack interaction effect on SIFs could be demonstrated by three categories. The first is the amplification or enhancement influence, which indicates that the normalized SIFs for two cracks are found to be higher than those of a single crack due to the crack interaction. The second type is the shielding effect, where due to the crack interaction, the normalized SIFs for the case of two cracks were found to be less than those of a single crack. The third category represents the case of no interaction between the cracks, where each crack could be treated as an isolated crack.

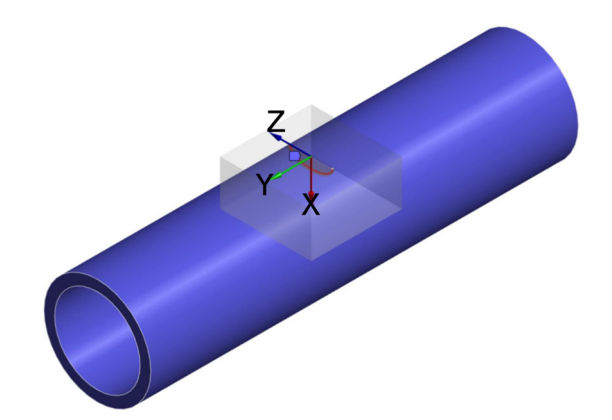


Fig. 5. Hollow cylinder with single crack with semi-elliptical crack setting.

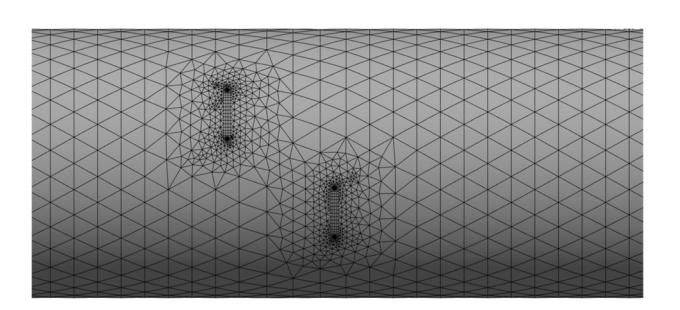


Fig. 6. Close view of the noncoplanar parallel crack configuration.

Based on the literature, for validation purposes, the commonly accepted rate of error between the two examined values must not exceed 5%, which is a commonly used value. Therefore, it has been assumed that the maximum difference between the obtained SIFs in the current study and the SIFs obtained in Ref. [33], must not exceed 5%. As depicted in Table III, where SIFs in terms of three values of crack aspect ratio (a/c) have been compared, each value of a/c examined for three values of the relative crack depth (a/t), the maximum error found between these results was equal to 4.10%. Based on the results in Table III, for a thin cylinder, the SIFs of the present model with a single circumferential crack under tension loading seem to be in good agreement with the SIFs of Ref. [33] for similar crack geometry.

TABLE III. CRACK VALIDATIONS

a/c		De	epest po	int	Sur	face Po	oint
a/C	a/t	0.2	0.5	0.8	0.2	0.5	0.8
	Reference [28]	1.097	1.167	1.247	0.930	1.070	1.290
0.6	Present	1.072	1.155	1.201	0.907	1.031	1.235
	Error (%)	2.27	1.02	3.68	2.47	3.64	4.26
	Reference [28]	1.057	1.101	1.144	1.051	1.156	1.335
0.8	Present	1.043	1.103	1.102	1.018	1.137	1.318
	Error (%)	1.32	-0.18	3.67	3.13	1.64	1.27
	Reference [28]	1.020	1.049	1.074	1.152	1.233	1.380
1.0	Present	1.028	1.3069	1.051	1.119	1.221	1.385
	Error (%)	-0.78	-1.90	2.14	2.86	0.97	-0.36

IV. RESULT AND DISCUSSION

The noncoplanar parallel crack configuration was examined when located on the external and internal surfaces of a thin cylinder. Where the distribution of the normalized SIFs, as well as the interaction factor, is presented as a function of the normalized crack front position under tension, bending, torsion, and mixed-mode loading. It should be noted that the overlapping angles between the cracks were not the same as that utilized for thick cylinders, whereas, for thin cylinders, the employed angles were 5°, 10°, and 15°. Due to the same trend presented by the overlapping angles, results for 5° are only presented due to its significant effect.

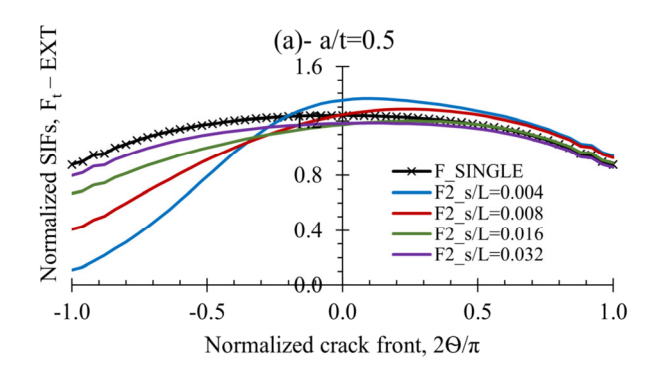
A. External Non-Coplanar Cracks under Tension

Fig. 7 illustrates the trend of the normalized SIFs for external noncoplanar parallel cracks under remote tension loading, F_{t-EXT} , for inclination angle $\alpha=5^{\circ}$, when a/c=0.4 for a/t=0.5 and 0.8. Due to cracks overlapping, the interaction between the cracks affected the overall curve shape of the F_{t-EXT} for the double cracks compared to F^{*}_{SINGLE} Where in the case of parallel cracks, the trend of the normalized SIFs for double parallel cracks followed an exact similar curve shape of $F_{_SINGLE}$ for all the examined s/L, despite the presence of interaction. However, the distribution of the noncoplanar parallel cracks configuration along the crack front was found to be asymmetric, compared to the symmetrical distribution

which was found in the case of parallel cracks. Also, the distribution of F_{t-EXT} for two cracks for all analyzed, s/L, demonstrated the amplification and shielding effect simultaneously.

Moreover, the F_{t-EXT} distribution displayed in Fig. 7 revealed that for a particular crack shape ratio, a/c, the relative depth of the crack, a/t, has a notable influence on the F_{t-EXT} value. Where the value of F_{t-EXT} when a/t = 0.5 was found to be less than that of a/t = 0.8 for the same aspect ratio, this impact was applicable for all the examined s/L ratios. On the other hand, the shielding effect occurs within the zone of overlapping or at one edge, while at the opposite region, the amplification effect was noticed between the cracks.

Additionally, the change in s/L ratio presented two unique trends in terms of the trend of the F_{t-EXT} depending on the position on the crack front, where in the zone of crack overlapping (half crack length), F_{t-EXT} increases with the increase of s/L and vice versa. While, from the deepest point on the crack front B and the second crack half, F_{t-EXT} increases with the decrease of s/L and vice versa.



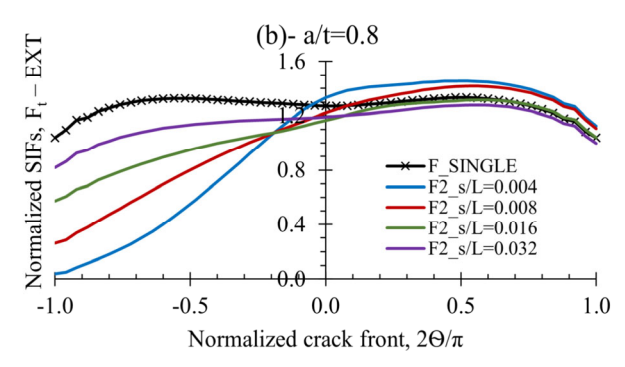


Fig. 7. The normalized SIFs for external noncoplanar parallel cracks under tension, for a thin cylinder, when $\alpha = 5^{\circ}$, a/c = 0.4, (a) a/t = 0.5, (b) a/t = 0.8.

Table IV shows the interaction factor Ψ , for external noncoplanar parallel cracks under tension loading when $\alpha=5^{\circ}$ and a/c=0.4. Generally, based on Eq. (2), it is obvious that Ψ displayed shielding and amplification effects along the crack front. Furthermore, for a/t=0.5, at points A and B, a slight interaction effect was noticed when s/L=0.004, and after s/L increases, Ψ showed no crack interaction influence, while at point C, an obvious shielding effect, where the shielding rate rises with the decline of the separation distance. On the other hand, for a/t=0.8, Ψ indicated that each of A, B, and C behaved

similarly to that of a/t = 0.5; however, the major difference was found in the rate of interaction influence.

TABLE IV. Interaction Factor for Noncoplanar Parallel External Cracks on Thin Cylinder under Tension $\alpha=5^\circ,\ a/c=0.4$

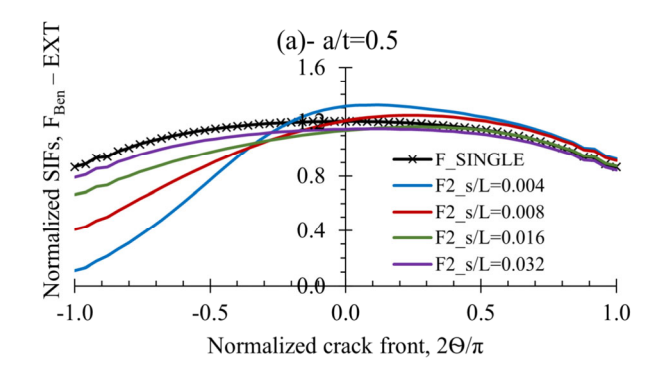
Interaction Factor, ψ	Point	s/L = 0.004	s/L = 0.008	s/L = 0.016	s/L = 0.032
6 /4	A	1.073	1.058	1.011	0.978
ψ for a/t =	В	1.090	1.004	0.947	0.954
0.5	C	0.124	0.465	0.762	0.910
6 /4	A	1.082	1.065	1.002	0.961
ψ for a/t =	В	1.048	0.959	0.916	0.936
0.8	C	0.035	0.251	0.551	0.787

Furthermore, for a/t=0.5, the maximum shielding effect was found at point C when s/L=0.004, where Ψ indicated that the SIFs for two noncoplanar parallel cracks under tension were about 88% less than $F_{_SINGLE}$. Similarly, for a/t=0.8, the maximum shielding influence was noticed at point C also, where Ψ revealed that SIFs for two noncoplanar parallel cracks under tension was about 97% less than $F_{_SINGLE}$, the difference between the two reduction ranges triggered to the high crack depth in the case of a/t=0.8. In addition, the maximum interaction effect, which has been remarked at point C, gradually decreases with the growth of the separation distance till approaching the largest examined distance s/L=0.032, where Ψ values implied the presence of the interaction influence since Ψ values at C are still less than 1.0.

B. External Non-Coplanar Cracks Under Bending

Fig. 8 illustrates the trend of the normalized SIFs for external noncoplanar parallel cracks under bending loading, $F_{Ben-EXT}$, for inclination angle $\alpha = 5^{\circ}$, when a/c = 0.4 for a/t = 0.5 and 0.8. Evidently, the distribution of the noncoplanar parallel cracks configuration along the crack front was found to be asymmetric. Besides, the distribution of F_{Ben-EXT} for two cracks for all analyzed s/L exhibited the amplification and shielding impact simultaneously. Moreover, F_{Ben-EXT} distribution shown in Fig. 8 revealed that a/t has a significant influence on a particular crack shape ratio, a/c, where the value of $F_{Ben-EXT}$ for a/t = 0.5 found to be less than that of a/t = 0.8, for the same aspect ratio, this impact was applicable for all the examined s/L ratios. On the other hand, the shielding effect occurs within the zone of overlapping or at one edge, while at the opposite region, the amplification effect was noticed between the cracks.

Table V illustrates the interaction factor Ψ , for external noncoplanar parallel cracks under bending loading when $\alpha = 5^{\circ}$ and a/c = 0.4. Furthermore, for a/t = 0.5, at points A and B, a slight interaction effect was noticed when s/L = 0.004 only, and after s/L expands, Ψ revealed no crack interaction impact, while at point C, an apparent shielding effect, where the shielding rate grows with the decline of the separation distance. On the other hand, for a/t = 0.8, Ψ indicated that each of A, B, and C behaved similarly to that of a/t = 0.5; however, the major difference was found in the rate of interaction influence.



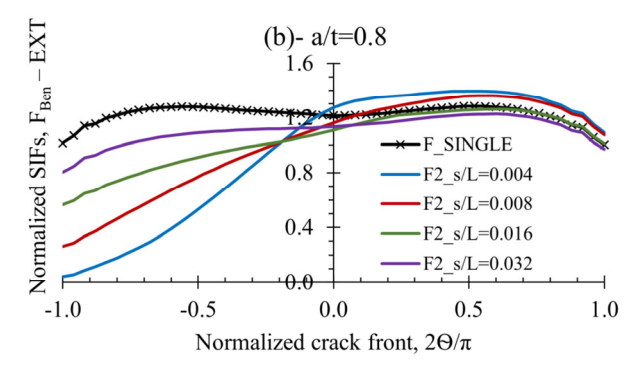


Fig. 8. The normalized SIFs for external noncoplanar parallel cracks under bending, for a thin cylinder, when $\alpha = 5^{\circ}$, a/c = 0.4, (a) a/t = 0.5, (b) a/t = 0.8.

TABLE V. Interaction Factor for Noncoplanar Parallel External Cracks on the Thin Cylinder under Bending when $\alpha=5^{\circ},\, a/c=0.4$

Interaction Factor, y	Point	s/L = 0.004	s/L = 0.008	s/L = 0.016	s/L = 0.032
_	A	1.068	1.054	1.007	0.974
ψ for a/t = 0.5	В	1.090	1.003	0.945	0.953
•	C	0.129	0.470	0.766	0.912
	A	1.088	1.071	1.008	0.967
ψ for a/t = 0.8	В	1.047	0.975	0.913	0.934
•	C	0.041	0.258	0.557	0.792

Additionally, for a/t = 0.5, the maximum shielding effect was found at point C when s/L = 0.004, where the reduction was about 88% less than that of $F_{_SINGLE}$. Likewise, for a/t = 0.8, the maximum shielding influence was noticed also at point C, when s/L = 0.004, where the reduction was about 96% less than of $F_{_SINGLE}$, the difference between the two reduction ranges caused by the high crack depth in the case of a/t = 0.8. In addition, the interaction influences in terms of amplification or shielding were found to be diminished with the growth of the separation distance s/L.

C. External Non-Coplanar Cracks Under Torsion

Fig. 9 explains the distribution of mode II normalized SIFs for external noncoplanar parallel cracks under torsion loading, $F_{\text{Tor-II-EXT}}$, for inclination angle $\alpha = 5^{\circ}$, when a/c = 0.4 for a/t = 0.5 and 0.8. Apparently, the distribution of the noncoplanar parallel cracks configuration along the crack front all analyzed s/L, exhibited the shielding impact only. Moreover, the shielding effect occurs within the area of overlapping, or at one edge, while at the opposite region, no interaction influence was noticed between the cracks. It

should be noted that, for mode II, the crack interaction influence remarked for $s/L \le 0.008$, the change in s/L beyond this range was found to be insensitive to the interaction influence rate.

TABLE VI. INTERACTION FACTOR FOR NONCOPLANAR PARALLEL EXTERNAL CRACKS ON THIN CYLINDER UNDER TORSION MODE II WHEN $\alpha=5^\circ$, a/c=0.4

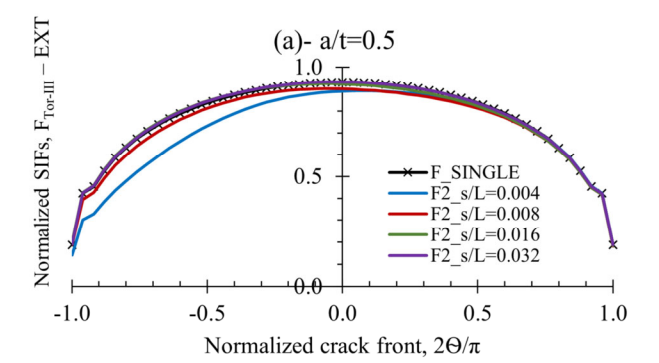
Interaction Factor, ψ	Point	s/L = 0.004	s/L = 0.008	s/L = 0.016	s/L = 0.032
ψ for a/t =	A	1.003	0.990	0.985	0.996
0.5	C	0.689	0.922	1.009	1.006
ψ for a/t =	A	1.011	0.987	0.970	0.985
0.8	C	0.552	0.800	0.969	1.015

Table VI clarifies the interaction factor Ψ , for external noncoplanar parallel cracks under torsion loading when $\alpha=5^\circ$ and a/c=0.4. It should be noted that based on the trend of $F_{Tor\text{-}II\text{-}EXT}$ along the crack front, the SIFs at the deepest point on the crack front were zero; therefore, Ψ for point B is not considered in Table VI. Moreover, no significant influence has been detected at point A for both a/t values with respect to all examined s/L, where Ψ implies that point A was sufficiently separated from the effect of the neighbor crack. On the other hand, at point C, for both examined a/t, the significant effect was more pronounced for $s/L \le 0.008$; for greater than this range, there was no remarkable impact.

As mentioned above, the shielding effect was noticed at point C, for a/t = 0.5 and 0.8, the maximum shielding was attained when s/L = 0.004 for both a/t ratios, but the reduction scale was different value of a/t. Additionally, for a/t = 0.5, Ψ showed about a 32% reduction in SIFs for the two noncoplanar parallel cracks case due to the shielding effect when compared to the F_{SINGLE} . Also, for a/t = 0.8, the maximum shielding influence was noticed at point C, where the reduction was about 45% less than that of F _{SINGLE}; the difference between the two reduction ranges was caused by the high crack depth in the case of a/t = 0.8. Besides, it was obvious that the interaction influence in terms of the shielding influence was found to be weakened with the growth of the separation distance s/L; this was more apparent in the case of torsion loading than in other types of loading.

Fig. 9 describes the distribution of mode III normalized SIFs for external noncoplanar parallel cracks under torsion loading, $F_{\text{Tor-III-EXT}}$, for inclination angle $\alpha = 5^{\circ}$, when a/c = 0.4 for a/t = 0.5 and 0.8.

Apparently, the distribution of the noncoplanar parallel cracks configuration along the crack front all studied s/L, displayed the shielding impact only. Moreover, the shielding effect appears within the vicinity of overlapping or at one edge, while at the opposite area, no interaction influence was noticed between the cracks. It should be noted that, for mode III, the crack interaction influence remarked for s/L ≤ 0.008 ; the change in s/L further than this range was found to be insensitive to the interaction influence rate.



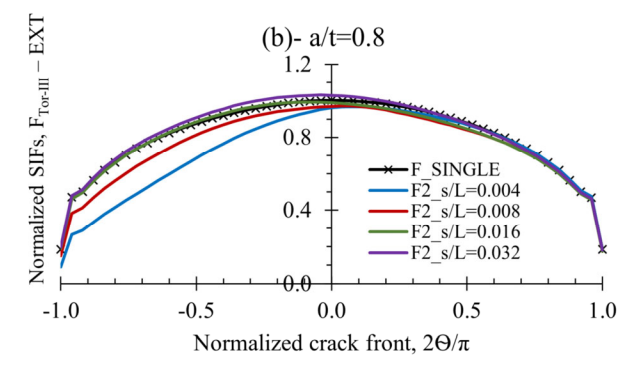


Fig. 9. The normalized SIFs for external noncoplanar parallel cracks under torsion mode III, for thin cylinder, when $\alpha = 5^{\circ}$, a/c = 0.4, (a) a/t = 0.5, (b) a/t = 0.8.

Table VII illuminates the interaction factor Ψ , for external noncoplanar parallel cracks under torsion loading when $\alpha=5^\circ$ and a/c=0.4. Moreover, no significant interaction influence has been identified at points A and B for both a/t values with respect to all examined s/L, where Ψ entailed that points A and B were adequately separated from the effect of the neighbor crack. On the other hand, at point C, the significant effect was noticed when s/L=0.004 for a/t=0.5, and for a/t=0.8, the effect was more evident for $s/L \le 0.008$; for greater than this range, there was no remarkable impact.

As mentioned, the shielding effect was noticed at point C, for a/t = 0.5 and 0.8, the highest shielding was attained when s/L = 0.004 for both a/t ratios, but the reduction amount was altered for each value of a/t. Additionally, for a/t = 0.5, Ψ showed about a 25% decrease in SIFs for the case of two noncoplanar parallel cracks due to the shielding effect when compared to the F SINGLE. Also, for a/t = 0.8, the maximum shielding influence was noticed at point C, where the drop was about 52% less than that of F _{SINGLE}, the difference between the two reduction ranges caused owing to the high crack depth utilized in the case of a/t = 0.8. Besides, it was obvious that the interaction influences in terms of the shielding were found to be diminished with the growth of the separation distance s/L, which was found to be more evident in the case of torsion loading than in other types of loading.

Fig. 10 describes the distribution of equivalent normalized SIFs for external noncoplanar parallel cracks under mixed-mode loading, $F_{EQV-EXT}$, for inclination angle $\alpha = 5^{\circ}$, when a/c = 0.4 for a/t = 0.5 and 0.8.

TABLE VII. Interaction Factor for Noncoplanar Parallel External Cracks on Thin Cylinder under Torsion Mode II when $\alpha=5^{\circ}$, a/c = 0.4

Interaction Factor, ψ	Point	s/L = 0.004	s/L = 0.008	s/L = 0.016	s/L = 0.032
6/4	A	0.990	0.973	0.979	0.998
$\psi \text{ for a/t} = 0.5$	В	0.956	0.968	0.992	1.002
	C	0.754	1.009	1.055	1.020
ψ for a/t =	A	0.987	0.947	0.940	0.974
	В	0.960	0.968	0.989	1.029
0.8	C	0.489	0.806	1.025	1.052

Obviously, due to crack interaction, the distribution of $F_{EQV-EXT}$ for noncoplanar parallel cracks configuration along the crack front was found to be asymmetric, besides the distribution of $F_{EQV-EXT}$ for two cracks for all analyzed s/L exhibited amplification and shielding impacts simultaneously. Furthermore, $F_{EQV-EXT}$ trend presented in Fig. 10 exposed that a/t has a noteworthy influence on certain crack shape ratio, a/c, where the value of $F_{EQV-EXT}$ for a/t = 0.5 found to be less than that of a/t = 0.8, for the same aspect ratio, this impact was valid for all the examined s/L ratios. On the other hand, the shielding effect arises within the overlapping zone or at one edge, while at the opposite region, the amplification effect is noticed between the cracks.

Table VIII demonstrates the interaction factor Ψ , for external noncoplanar parallel cracks under mixed-mode loading when $\alpha=5^{\circ}$ and a/c=0.4. Additionally, for a/t=0.5, at points A and B, feeble amplification interaction impact has been detected when s/L=0.004 only, and after s/L enlarges, Ψ implies no crack interaction effect, while at point C, an apparent shielding effect was noticed, where the shielding rate produces with the decrease of the separation distance. On the other hand, for a/t=0.8, Ψ indicated that each of A, B, and C behaved similarly to that displayed by a/t=0.5; however, the main difference was found in the rate of interaction influence.

Also, for a/t = 0.5, the greatest shielding effect was observed at point C when s/L = 0.004, where the reduction was about 87% less than that of F_{SINGLE} . Similarly, for a/t = 0.8, the strongest shielding influence is also seen at point C, when s/L = 0.004, where the reduction was about 84% less than of F_{SINGLE} , the difference in the crack depth between the two cases caused the discrepancy between the reduction scales.

D. Internal Non-Coplanar Cracks Under Tension

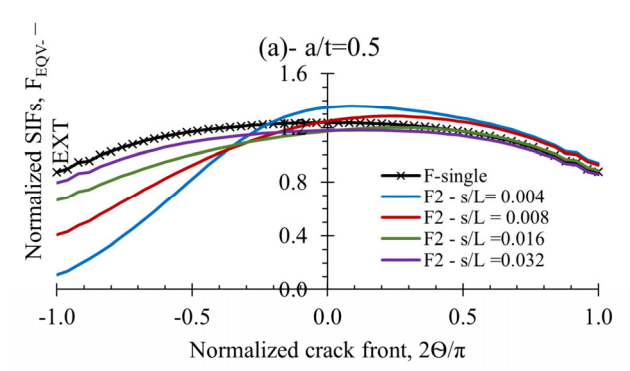
Fig. 11 illustrates the trend of the normalized SIFs for internal noncoplanar parallel cracks under tension loading, F_{t-INT} , for inclination angle $\alpha=5^{\circ}$, when a/c=0.4 for a/t = 0.5 and 0.8.

Generally, the allocation of F_{t-INT} for noncoplanar parallel cracks configuration along the crack front was found to be asymmetric, besides the distribution of F_{t-INT} for two cracks for all the analyzed s/L exhibited shielding impact only. The F_{t-INT} distribution in Fig. 11 also revealed that a/t has a substantial influence on certain crack shape ratio, a/c, where the value of F_{t-INT} for a/t = 0.5 found to be less than that of a/t = 0.8, for the same aspect ratio, this impact was appropriate for all the examined s/L ratios. Also, the shielding effect occurs within the zone of

overlapping, or at one edge, while at the opposite region, no practical effect is noticed between the cracks.

TABLE VIII. Interaction Factor for Noncoplanar Parallel External Cracks on Thin Cylinder under Mixed Mode when $\alpha=5^\circ$, a/c = 0.4

Interaction Factor, ψ	Point	s/L = 0.004	s/L = 0.008	s/L = 0.016	s/L = 0.032
vy for alt -	Α	1.072	1.058	1.012	0.978
ψ for a/t =	В	1.092	1.009	0.949	0.955
0.5	C	0.130	0.466	0.762	0.910
6/4	A	1.082	1.066	1.005	0.963
ψ for a/t =	В	1.052	0.964	0.920	0.937
0.8	C	0.167	0.285	0.965	0.798



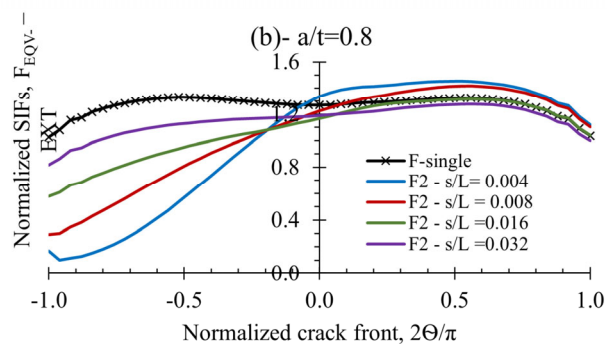
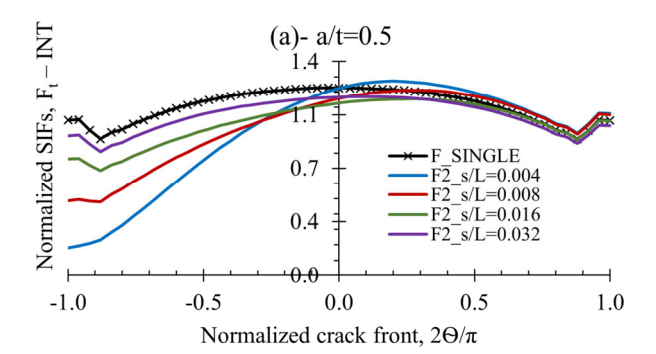


Fig. 10. The normalized SIFs for external non-coplanar parallel cracks under mixed mode, for thin cylinder, when $\alpha=5^{\circ}$, a/c = 0.4, (a) a/t = 0.5, (b) a/t = 0.8.

Table IX reveals the interaction factor Ψ , for internal noncoplanar parallel cracks under tension loading when $\alpha=5^{\circ}$ and a/c=0.4. Moreover, for a/t=0.5, at points A and B, minor interaction influence was detected, but the severe interaction impact was noticed at point C, which was demonstrated by the shielding effect; this was applicable for all examined s/L. On the other hand, for a/t=0.8, Ψ indicated that each of B and C experienced shielding influence, where the maximum effect was noticed at point C.

Generally, for a/t = 0.8, it has been found that the interaction influence (either amplification or shielding) of the internal noncoplanar parallel cracks under tension loading for all examined a/c ratios, higher than those of external noncoplanar parallel cracks, which was applicable to all examined s/L ratios. While, for a/t = 0.5, the behavior was found to be the same, but with a slight difference between the two considered cases. Also, the maximum shielding effects noticed at point C for both examined a/t values, where SIFs for two cracks were reduced by 83%

for a/t = 0.5 and about 91% reduction at the same point for a/t = 0.8, the difference in the interaction rate caused by the high crack depth employed in a/t = 0.8.



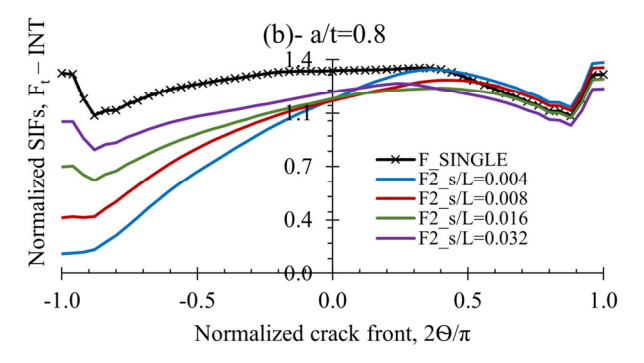


Fig. 11. The normalized SIFs for internal noncoplanar parallel cracks under tension, for a thin cylinder, when $\alpha = 5^{\circ}$, a/c = 0.4, (a) a/t = 0.5, (b) a/t = 0.8.

Table IX. Interaction Factor for Noncoplanar Parallel Internal Cracks on Thin Cylinder under Tension when $\alpha=5^{\circ},~a/c=0.4$

Interaction Factor, ψ	Point	s/L = 0.004	s/L = 0.008	s/L = 0.016	s/L = 0.032
	A	1.046	1.039	0.997	0.966
ψ for a/t = 0.5	В	0.999	0.943	0.919	0.951
	C	0.176	0.479	0.747	0.899
$\psi \text{ for a/t} = 0.8$	Α	1.059	1.034	0.977	0.927
	В	0.858	0.852	0.863	0.896
	C	0.099	0.276	0.532	0.757

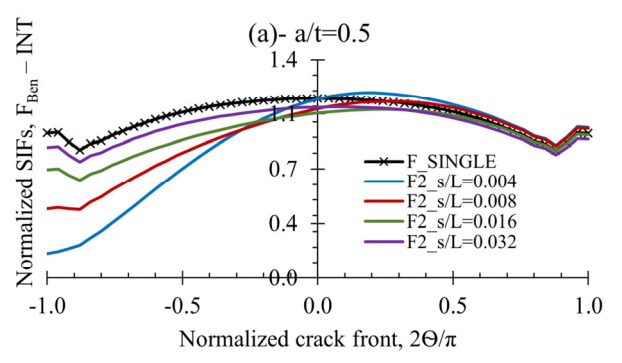
E. Internal Non-Coplanar Cracks Under Bending

Fig. 12 illustrates the trend of the normalized SIFs for internal noncoplanar parallel cracks under bending loading, $F_{Ben-INT}$, for inclination angle $\alpha = 5^{\circ}$, when a/c = 0.4 for a/t = 0.5 and 0.8.

Mostly, due to the crack interaction, the trend of $F_{Ben-INT}$ for noncoplanar parallel cracks configuration along the crack front was found to be asymmetric, besides the distribution of $F_{Ben-INT}$ for two cracks for all the analyzed s/L displayed shielding effect only. The $F_{Ben-INT}$ distribution in Fig. 12 also showed that a/t has a substantial influence on certain crack shape ratio, a/c, where the value of $F_{Ben-INT}$ for a/t = 0.5 found to be less than that of a/t = 0.8, for the same aspect ratio, this impact was correct for all the examined s/L ratios. Also, the shielding effect appears within the zone of overlapping or at one edge, while at the opposite region, no reasonable effect is noticed between the cracks.

Table X demonstrates the interaction factor Ψ , for internal noncoplanar parallel cracks under bending loading when $\alpha = 5^{\circ}$ and a/c = 0.4. Moreover, for a/t = 0.5, at points A and B, a slight interaction influence was detected. However, the severe interaction impact was noticed at point C, which was proven by the shielding effect; this was applicable for all examined s/L. On the other hand, for a/t = 0.8, Ψ implied that each of B and C experienced shielding influence, where the maximum effect was noticed at point C.

Largely, for a/t = 0.8, it has been found that the interaction influence (both amplification and shielding) of the internal noncoplanar parallel cracks under bending loading for all examined a/c ratios, higher than those of external noncoplanar parallel cracks, which was applicable to all examined s/L ratios. For a/t = 0.5, the behavior was found to be the same, but with a minor difference between the two considered cases. Also, the maximum shielding effects noticed at point C for both examined a/t values, where SIFs for two cracks were reduced by 83% for a/t = 0.5 and about 91% reduction at the same point for a/t = 0.8, the difference in the interaction rate caused by the high crack depth employed in a/t = 0.8.



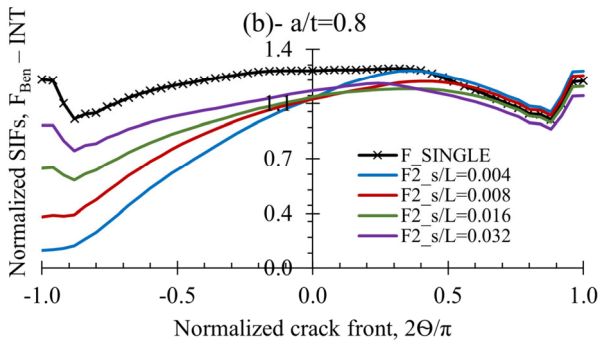


Fig. 12. The normalized SIFs for internal noncoplanar parallel cracks under bending, for a thin cylinder, when $\alpha = 5^{\circ}$, a/c = 0.4, (a) a/t = 0.5, (b) a/t = 0.8.

Table X. Interaction Factor for Noncoplanar Parallel Internal Cracks on Thin Cylinder under Bending when $\alpha=5^{\circ}$, a/c = 0.4

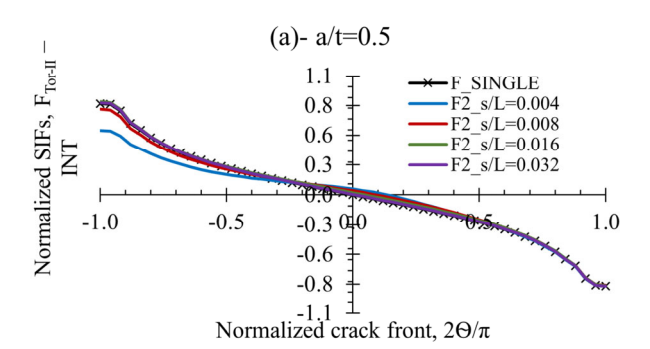
Interaction Factor, ψ	Point	s/L = 0.004	s/L = 0.008	s/L = 0.016	s/L = 0.032
	A	1.042	1.035	0.992	0.961
ψ for a/t = 0.5	В	0.998	0.943	0.919	0.951
	C	0.172	0.477	0.748	0.901
	A	1.054	1.028	0.970	0.920
ψ for a/t = 0.8	В	0.859	0.854	0.865	0.897
Y	C	0.096	0.273	0.531	0.758

F. Internal Non-Coplanar Cracks under Torsion

Fig. 13 explains the tendency of the mode II normalized SIFs for internal noncoplanar parallel cracks under torsion loading, $F_{Tor-II-INT}$, for inclination angle $\alpha = 5^{\circ}$, when a/c = 0.4 for a/t = 0.5 and 0.8.

Mainly, due to the interaction between the cracks, the tendency of F_{Tor-II-INT} for noncoplanar parallel cracks configuration along the crack front was found to be asymmetric, besides the distribution of F_{Tor-II-INT} for two cracks for all the analyzed s/L, displayed shielding effect only. Also, the shielding effect appears within the zone of overlapping or at one edge, while at the opposite region, no reasonable effect is noticed between the cracks.

The interaction factor Ψ, for internal noncoplanar parallel cracks under torsion loading, when $\alpha = 5^{\circ}$ and a/c = 0.4, is demonstrated in Table XI. It should be noted that due to the $F_{Tor-II-INT}$ distribution, where $F_{Tor-II-INT} = 0$ at point B, therefore, point B was not mentioned in the table. Moreover, no significant interaction influence has been noticed at point A for both examined a/t ratios, even though the major interaction impact was observed at point C, which was demonstrated by the shielding effect and was applicable for all examined s/L.



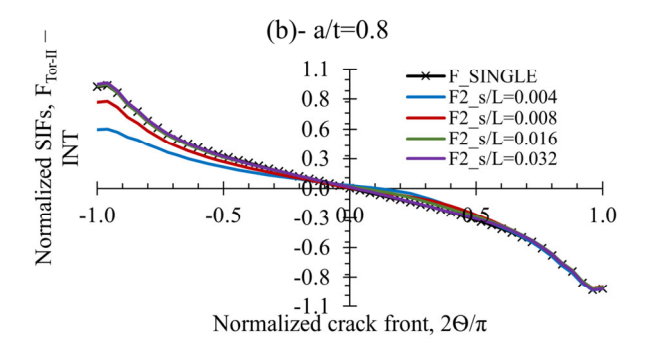


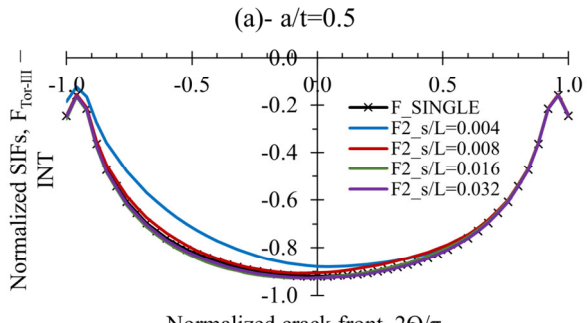
Fig. 13. The normalized SIFs for internal noncoplanar parallel cracks under torsion mode II, for thin cylinder, when $\alpha = 5^{\circ}$, a/c = 0.4, (a) a/t = 0.5, (b) a/t = 0.8.

As depicted in Table XI, Y showed that for mode II torsion loading, the cracks require small separation distances to be separated or isolated from the neighbor crack effect. Moreover, at point C, since there was no influence at point A, for both examined ratios, the interaction influence was detected only for s/L ≤0.008. where Ψ beyond this limit, displayed no significant interaction influence. Also, the maximum shielding effect observed at point C for both examined a/t values, where SIFs for two cracks reduced by 30% for a/t = 0.5, and about 42% reduction at the same point for a/t = 0.8, the difference in the interaction rate caused by the high crack depth employed in a/t = 0.8.

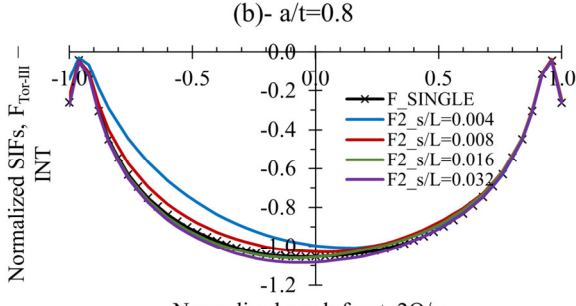
TABLE XI. INTERACTION FACTOR FOR NONCOPLANAR PARALLEL INTERNAL CRACKS ON THIN CYLINDER UNDER TORSION MODE II WHEN $\alpha = 5^{\circ}$, a/c = 0.4

Interaction Factor, w	Point	s/L = 0.004	s/L = 0.008	s/L = 0.016	s/L = 0.032
ψ for a/t =	Α	1.000	0.991	0.995	1.001
0.5	C	0.703	0.938	1.022	1.009
ψ for a/t =	Α	1.002	0.978	0.982	1.001
0.8	C	0.583	0.850	1.011	1.025

Fig. 14 describes the trend of the mode III normalized SIFs for internal noncoplanar parallel cracks under torsion loading, $F_{Tor-III-INT}$, for inclination angle $\alpha = 5^{\circ}$, when a/c = 0.4 for a/t = 0.5 and 0.8. Principally, the distribution of F_{Tor-III-INT} implies that, under mode III torsion loading, internal circumferential behaved the opposite to that of external cracks under the same type of loading. This indicates the probability of crack propagation under mode III torsion loading for external cracks is higher than that of internal cracks. Despite this opposite distribution nature, crack interaction influence was found to be in the form of an amplification effect, which was found to be more pronounced when s/L = 0.004 for both a/t ratios; otherwise, no significant interaction influence has been remarked. Also, the crack interaction influence appears within the zone of overlapping or at one crack edge, while at the opposite region, no sensible effect is noticed between the cracks.



Normalized crack front, $2\Theta/\pi$



Normalized crack front, $2\Theta/\pi$

Fig. 14. The normalized SIFs for internal noncoplanar parallel cracks under torsion mode III, for thin cylinder, when $\alpha = 5^{\circ}$, a/c = 0.4, (a) a/t = 0.5, (b) a/t = 0.8.

TABLE XII. Interaction Factor for Noncoplanar Parallel Internal Cracks on the Thin Cylinder under Torsion Mode III when $\alpha=5^{\circ}$, a/c = 0.4

Interaction Factor, ψ	Point	s/L = 0.004	s/L = 0.008	s/L = 0.016	s/L = 0.032
	A	0.986	0.976	0.991	1.003
ψ for a/t = 0.5	В	0.954	0.984	1.006	1.007
'	C	0.756	1.001	1.054	1.019
	Α	0.968	0.933	0.962	1.005
ψ for a/t = 0.8	В	0.947	0.976	1.003	1.028
	C	0.544	0.887	1.069	1.060

The interaction factor Ψ , for internal noncoplanar parallel cracks under torsion loading, when $\alpha=5^\circ$ and a/c=0.4, is demonstrated in Table XI. Moreover, no significant interaction influence has been noticed at points A and B for both examined a/t ratios, even though the major interaction influence was observed at point C, which was clarified by the shielding effect. As illustrated in Table XII, Ψ showed that for mode III torsion loading, the cracks require small separation distances to be separated or isolated from the neighbor crack effect. Also, at point C, the interaction influence was detected only for $s/L \le 0.008$, for a/t=0.8, while for a/t=0.5, the interaction influence was noticed when s/L=0.004 only, where Ψ beyond this limit, displayed no significant influence.

Additionally, the maximum shielding effect observed at point C for both examined a/t values was found to be different depending on the examined crack depth; therefore, the SIFs for the case of two cracks reduced by 25% for a/t = 0.5, and about 46% reduction at the same point for a/t = 0.8. Fig. 15 explains the trend of the equivalent normalized SIFs for internal noncoplanar parallel cracks under mixed-mode loading, $F_{EQV-INT}$, for inclination angle $\alpha = 5^{\circ}$, when a/c = 0.4 for a/t = 0.5 and 0.8.

TABLE XIII. Interaction Factor for Noncoplanar Parallel Internal Cracks on the Thin Cylinder under Mixed Mode when $\alpha=5^{\circ}$, a/c = 0.4

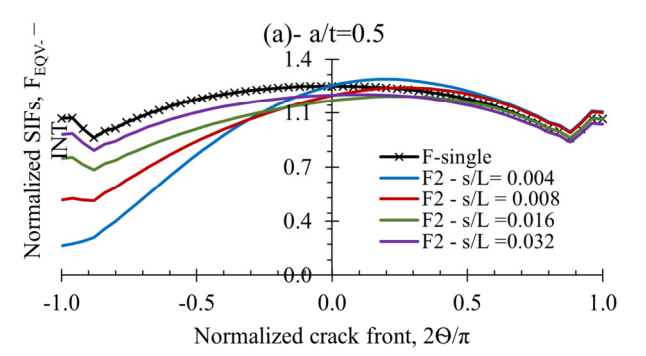
Interaction Factor, ψ	Point	s/L = 0.004	s/L = 0.008	s/L = 0.016	s/L = 0.032
$\psi \text{ for a/t} = 0.5$	A	1.046	1.040	0.999	0.967
	В	1.004	0.950	0.922	0.952
	C	0.188	0.481	0.747	0.899
ψ for a/t = 0.8	Α	1.060	1.035	0.981	0.926
	В	0.860	0.856	0.867	0.898
	C	0.116	0.279	0.535	0.758

Mostly, due to the crack interaction, the trend of $F_{EQV-INT}$ for noncoplanar parallel cracks configuration along the crack front was found to be asymmetric, and the distribution of $F_{EQV-INT}$ for two cracks for all the analyzed s/L displayed a shielding effect only. The $F_{EQV-INT}$ distribution in Fig. 15 indicated that a/t has considerable influence on the specific crack shape ratio, a/c, where the value of $F_{EQV-INT}$ for a/t = 0.5 was found to be less than that of a/t = 0.8 was, for the same aspect ratio, this impact was true for all examined s/L ratios. Moreover, the shielding effect exists inside the zone of overlapping or at one crack edge, while at the opposite zone, no sensible effect is observed between the cracks.

Table XIII presents the interaction factor Ψ , for internal noncoplanar parallel cracks under mixed-mode loading when $\alpha = 5^{\circ}$ and a/c = 0.4. Additionally, for a/t = 0.5, at points A and B, minor interaction influence was detected, although the severe interaction influence was noticed at point C, which was exhibited by the shielding effect; this was appropriate for all examined s/L. On the other hand, for a/t = 0.8, Ψ indicated that each of B and C experienced shielding influence, where the maximum effect was also noticed at point C.

Broadly, for a/t = 0.8, it has been found that the interaction influence (both amplification and shielding) of the internal noncoplanar parallel cracks under tension loading for all examined a/c ratios, higher than those of external noncoplanar parallel cracks, which was applicable to all examined s/L ratios. While, for a/t = 0.5, the behavior was found to be consistent, but with slightly lower differences between the two considered cases.

Also, the maximum shielding effect observed at point C for both examined a/t values, where SIFs for two cracks reduced by 82% for a/t = 0.5, and about 89% reduction at the same point for a/t = 0.8, the difference in the interaction rate caused by the high crack depth employed in a/t = 0.8. The Ψ value in Table XIII, for point C, implied that the interaction influence between the cracks still exists despite the large separation distance between the cracks, where for a/t = 0.5, when s/L = 0.032, SIFs for the two crack cases was 11% lower than that of $F_{_SINGLE}$, also for a/t = 0.8, SIFs was about 25% less than $F_{_SINGLE}$.



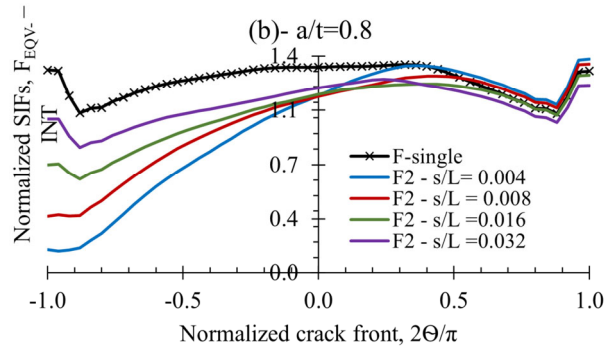


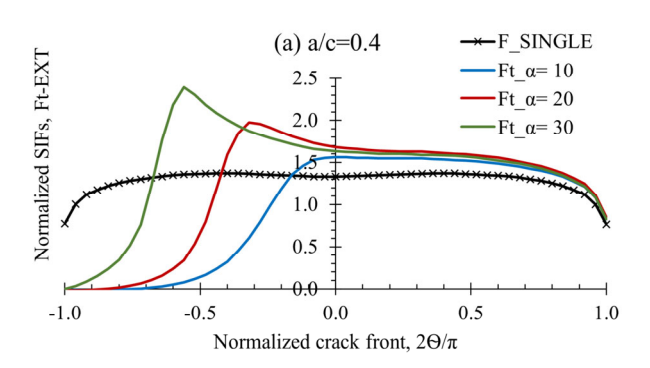
Fig. 15. The normalized SIFs for internal noncoplanar parallel cracks under mixed mode, for thin cylinder, when $\alpha = 5^{\circ}$, a/c = 0.4, (a) a/t = 0.5, (b) a/t = 0.8.

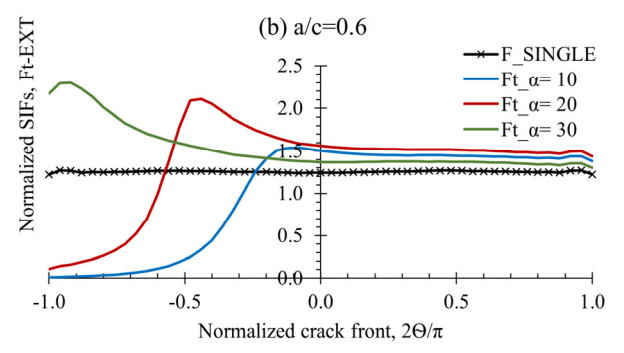
G. Effect of Inclination Angle on Crack Interactions

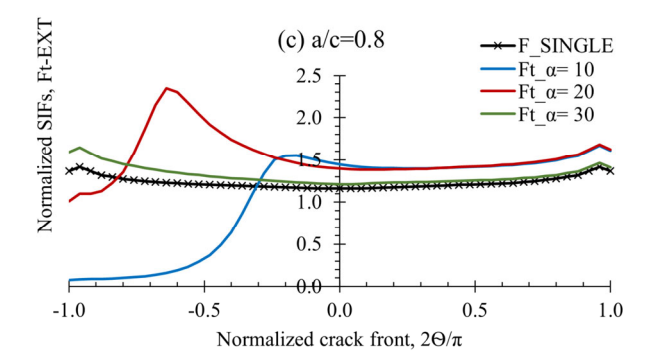
As mentioned before, the noncoplanar parallel crack configuration has been analyzed when located on the external and internal surfaces of thick and thin cylinders, under different types of loading. For each type of considered cylinder, the inclination angle of the cracks was defined separately, where for thick cylinder, $\alpha=10^\circ, 20^\circ,$ and 30° , while for thin cylinder, the considered inclination angle, $\alpha=5^\circ, 10^\circ,$ and $15^\circ.$ In the previous section, the distribution of normalized SIFs along the crack front for different types of loading have been presented for only one inclination angle, $\alpha=10^\circ$ for thick cylinders and $\alpha=5^\circ$ for thin cylinders.

To visualize the relationship between the inclination angle and the normalized SIFs in terms of crack interaction, it is necessary to present the SIFs as a function of the inclination angle (or could be used as the overlapping angle). Based on the results presented in the previous section, it has been found that the maximum interaction influence is attained always when s/L = 0.004 and a/t = 0.8. Where s/L = 0.004 demonstrates the smallest separation distance between the cracks, while a/t = 0.8, represents the deepest relative crack depth ratio. Therefore, the separation distance s/L = 0.004, as well as a/t = 0.8, have been selected to present the effect of inclination angle on the distribution of the normalized SIFs since both ratios produced the maximum interaction influence.

Fig. 16 shows the influence of different inclination angles on the distribution of the normalized SIFs as a function of the crack aspect ratio, a/c, under remote tension loading for external noncoplanar parallel cracks configuration located on the thick cylinder, when s/L = 0.004 and a/t = 0.8. Furthermore, to include a wide variety of crack shapes, the crack aspect ratio is varied from 0.4 to 1.2, which have been presented in Fig. 16, respectively. Also, the considered inclination angles, $\alpha = 10^{\circ}$, 20° and 30° .







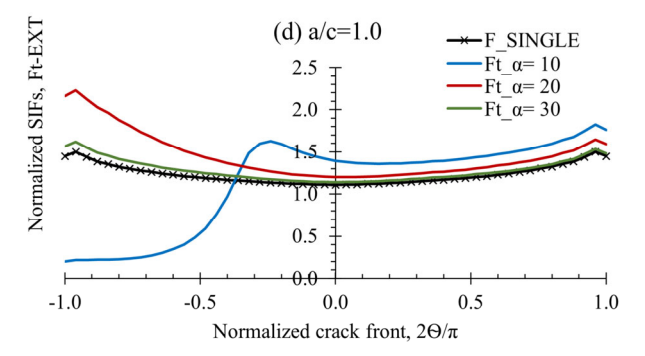


Fig. 16. The effect of inclination angle on SIFs for external cracks located on thick cylinder under tension loading for different aspect ratios.

Obviously, the inclination angle α has a significant influence on crack interaction behavior, and this effect strongly depends on the examined a/c, which has produced different impacts. The increase in a/c ratio is accompanied by the decrease in the F_{t-EXT} , which indicates that sharp cracks are risky or serious more than transverse cracks, where the highest F_{t-EXT} is attained when a/c = 0.4, while the minimum when a/c = 1.2.

On the other hand, α produced unique behaviors, depending on the examined a/c. Moreover, for $\alpha=10^\circ,$ $F_{t\text{-EXT}}$ distribution followed an approximately similar trend along the crack front with respect to the change in a/c, where the amplification effect was noticed in the region from $2\Theta/\pi=-0.2$ to 1.0 on the crack front, and the shielding effect recognized from $2\Theta/\pi=-0.2$ to -1, this effect was applicable to all examined a/c ratios, where with the increase of a/c, the area which experience the amplification impact increase also.

Also, for $\alpha=20^\circ$, F_{t^-EXT} distributed in two different styles; for a/c <1.0, F_{t^-EXT} exhibited both amplification and shielding effects along the crack front, whilst for a/c ≥1.0, a severe amplification effect was noticed in the overlapping zone, and minor amplification impact observed far away from the overlapping zone. It should be noted that during the change in a/c from 0.8 to 1.0 for $\alpha=20^\circ$, the F_{t^-EXT} behavior switched from the shielding and amplification mixed behavior to the pure amplification impact.

Similarly, for $\alpha=30^\circ$, it has been found that for this inclination angle, the influence on the $F_{t\text{-EXT}}$ distribution was more pronounced for a/c \leq 0.8, where it presented both interaction influences amplification and shielding. It should be noted that throughout the change in a/c from 0.4 to 0.6 for $\alpha=30^\circ$, the $F_{t\text{-EXT}}$ behavior converted from the

shielding and amplification mixed behavior to the pure amplification impact. Moreover, for a/c \geq 1.0, the inclination angle $\alpha = 30^{\circ}$ has no significant influence on the distribution of F_{t-EXT} along the crack front.

It is noteworthy that the change in the inclination angle under bending and mixed-mode loading behaved in the same manner that has been shown by tension loading. However, crack interaction in the tension loading case presented SIF values higher than those of other types of loading. Also, in the case of torsion loading, the effect of overlapping angle change is found to be insignificant with respect to tension, bending, and mixed-mode loading. In addition, the effect of the inclination angle on the crack interaction for internal cracks in a thick cylinder is found to be the same as that shown by external cracks. However, in the case of internal cracks, the rate of the amplification impact on the cracks due to the interaction was observed to be less than that detected in the external cracks case. This leads to the emphasis that interaction between double-surface cracks located on the external surface is considered riskier than the same cracks located on the internal surface under the same type of loading.

Typical behavior has been observed for the case of a thin cylinder when comparing the distribution of the normalized SIFs under any type of loading for the considered inclination angles. Moreover, external cracks located on thin cylinders under any of the examined types of loading presented an amplification impact rate higher than that of internal cracks. Which is again, another indicator of the significance of the external cracks.

V. CONCLUSION

In this work, the ANSYS finite element program is used to model and analyze cracks located internally and externally on the surfaces of the thin cylinders under various loading. Previously, a tremendous number of works dealing with singles were available. However, for the cases of multiple cracks, the number of papers is limited. The study of cracks in thin cylinders contributed to the study of component reliability, especially in the nuclear or oil and gas sector. From this study, conclusions are drawn according to their loading. Under tension force, normalized SIFs for double parallel cracks follow a similar trend despite interaction effects, exhibiting an asymmetric distribution with amplification and shielding. While under bending moment, crack depth (a/t ratio) significantly influences SIF values, with deeper cracks experiencing higher stress, shielding in overlapping regions, and amplification elsewhere. Under torsion, only shielding occurs, particularly in overlapping zones, while crack interaction weakens as separation distance (s/L) increases. A similar asymmetric pattern appears in tension and bending, where shielding effects dominate. Shielding remains prominent in torsion (Mode II and III), and interaction effects decrease as cracks move farther apart. Internal cracks exhibit lower amplification than external ones, making external cracks more critical for structural integrity. Additionally, the inclination angle strongly affects crack interaction, with external cracks in thin cylinders experiencing greater amplification and posing a

higher risk than internal cracks. The study of both single and multiple cracks, especially on the surface of a thin cylinder, is paramount to analyze the reliability of the component containing cracks and, therefore, prevent premature failure.

CONFLICT OF INTEREST

The authors declare no conflict of interest.

AUTHOR CONTRIBUTIONS

OMA-M conducted the research and analyzed the data; AEI drafted the paper; ZA drafted and final checked the paper; all authors had approved the final version.

FUNDING

This research was supported by Universiti Tun Hussein Onn Malaysia (UTHM) through Tier 1 (Vot Q497).

ACKNOWLEDGMENT

All authors wish to thank Universiti Tun Hussein Onn Malaysia for providing research facilities such as ANSYS finite element analysis software.

REFERENCES

- [1] D. Amato, L. E. Federico Armentani *et al.*, "Limits of applicability of LEFM: Numerical investigation on the crack-tip-yielding in a hollow-cylindrical specimen," *Procedia Structural Integrity*, vol. 52, pp. 1–11, 2024.
- [2] B. Abazadeh and A. Narjabadifam, "Several cracks in an orthotropic hollow cylinder coated by an MEE layer under torsion," *Theoretical and Applied Fracture Mechanics*, vol. 122, 103606, 2022
- [3] Z. Shen, C. Chen H. Xuan *et al.*, "Study on multiple fatigue cracks growth in the web of a hollow compressor impeller," *Engineering Fracture Mechanics*, vol. 292, 109582, 2023.
- [4] K. Yuan, K. Dong, Q. Fang et al., "Weight function and stress intensity factors for external circumferential surface cracks with high aspect ratio in cylinders," *International Journal of Pressure* Vessels and Piping, vol. 212, 105331, 2024.
- [5] D. F. Mora and M. Niffenegger, "A new simulation approach for crack initiation, propagation and arrest in hollow cylinders under thermal shock based on XFEM," *Nuclear Engineering and Design*, vol. 386, 111582, 2022.
- [6] C. Q. Li and S. T. Yang, "Stress intensity factors for high aspect ratio semi-elliptical internal surface cracks in pipes," *International Journal of Pressure Vessel and Piping*, vol. 96–97, pp. 13–23, 2012.
- [7] A. T. Diamantoudis and G. N. Labeas, "Stress intensity factors of semielliptical surface cracks in pressure vessels by global-local finite element methodology," *Engineering Fracture Mechanics*, vol. 72, no. 9, pp. 1299–1312, 2005.
- [8] K. J. Kirkhope, R. Bell, and J. Kirkhope, "Stress intensity factors for single and multiple semi-elliptical surface cracks in pressurized thick-walled cylinders," *International Journal of Pressure Vessel* and Piping, vol. 47, no. 2, pp. 247–257, 1991.
- [9] M. Kamaya, "A combination rule for circumferential surface cracks on pipe under tension based on limit load analysis," *International Journal of Pressure Vessel and Piping*, vol. 133, 021205, 2011.
- [10] R. Ghajar and S. M. Nabavi, "Closed-form thermal stress intensity factors for an internal circumferential crack in a thick-walled cylinder," Fatigue and Fracture of Engineering Materials and Structures, vol. 33, no. 8, pp. 504–512, 2010.
- [11] O. A. Terfas, A. M. Kraima, and R. B. Arieby, "Finite element analysis based stress intensity factor solutions for surface cracks," *International Journal of Engineering and Information Technology*, vol. 6, no. 1, pp. 22–28, 2019.

- [12] A. Carpinteri, "Shape change of surface cracks in round bars under cyclic axial loading," *International Journal of Fatigue*, vol. 15, no. 1, pp. 21–26, 1993.
- [13] M. da Fonte and M. de Freitas, "Stress intensity factors for semielliptical surface cracks in round bars under bending and torsion," *International Journal of Fatigue*, vol. 21, no. 5, pp. 457–463, 1999.
- [14] M. de Fonte, E. Gomes, and M. de Freitas, "Stress intensity factors for semielliptical surface cracks in round bars subjected to mode I (bending) and mode III (torsion) loading," *European Structural Integrity Society*, vol. 25, pp. 249–260, 1999.
- [15] A. E. Ismail, A. K. Ariffin, S. Abdullah et al., "Stress intensity factors under combined bending and torsion moments," *Journal of Zhejiang University Science A*, vol. 13, no. 1, pp. 1–8, 2012.
- [16] A. E. Ismail, A. K. Ariffin, S. Abdullah et al., "Stress intensity factors under combined tension and torsion loadings," *Indian Journal of Engineering and Material Science*, vol. 19, pp. 5–16, 2012.
- [17] C. S. Shin and C. Q. Cai, "Experimental and finite element analyses on stress intensity factors of an elliptical surface crack in a circular shaft under tension and bending," *International Journal of Fracture*, vol. 129, no. 3, pp. 239–264, 2004.
- [18] D. K. L. Tsang, S. O. Oyadiji, and A. Y. T. Leung, "Multiple penny-shaped cracks interaction in a finite body and their effect on stress intensity factor," *Engineering Fracture Mechanics*, vol. 70, no. 15, pp. 2199–2214, 2003.
- [19] M. K. Awang, A. E. Ismail, A. L. M. Tobi et al., "Stress intensity factors and interaction of two parallel surface cracks on cylinder under tension," in *Proc. IOP Conf. Series: Materials Science and Engineering*, 2017, vol. 165, 12009.
- [20] K. J. Kirkhope, R. Bell, and J. Kirkhope, "Stress intensity factors for single and multiple semi-elliptical surface cracks in pressurized thick-walled cylinders," *International Journal of Pressure Vessel* and Piping, vol. 47, no. 2, pp. 247–257, 1991.
- [21] D. S. Kim and K. H. Lo, "Crack interaction criteria in pressure vessels and pipe," *Journal of Offshore Mechanics and Arctic Engineering*, vol. 117, no. 4, pp. 260–264, 1995.
- [22] M. Perl, C. Levy, and J. Pierola, "Three-dimensional interaction effects in internally multicracked pressurized thick-walled cylinder. Part 1: Radial crack arrays," *Journal of Pressure Vessel Technology*, vol. 118, no. 3, pp. 357–363, 1996.
- [23] C. Levy, M. Perl, and N. Kokkavessis, "Three-dimensional interaction effects in an internally multicracked pressurized thickwalled cylinder-Part II: Longitudinal coplanar crack arrays,"

- Journal of Pressure Vessel Technology, vol. 118, no. 3, pp. 364–368, 1996.
- [24] C. Guozhong, J. Xianfeng, and L. Gan, "Analyses on interaction of internal and external surface cracks in a pressurized cylinder by hybrid boundary element method," *International Journal of Pressure Vessel and Piping*, vol. 81, no. 5, pp. 443–449, 2004.
- [25] R. G. Forman, J. C. Hickman, and V. Shivaskumar, "Stress intensity factors for circumferential through cracks in hollow cylinders subjected to combined tension and bending loads," *Engineering Fracture Mechanics*, vol. 21, no. 3, pp. 563–571, 1985.
- [26] J. S. J. Lyell, "Circumferential through-cracks in cylindrical shells under tension," *Journal of Applied Mechanics*, vol. 49, no. 1, pp. 103–107, 1982.
- [27] X. M. Kong, S. T. Zheng, and Z. Y. Cui, "Studies on stress intensity factor KI of surface cracks in a cylinder under remote tension loads," *Engineering Fracture Mechanics*, vol. 33, no. 1, pp. 105– 111, 1989.
- [28] C. Guozhong, Z. Kangda, and W. Dongdi, "Stress intensity factors for internal semi-elliptical surface cracks in pressurized thickwalled cylinders using the hybrid boundary element method," *Engineering Fracture Mechanics*, vol. 52, no. 6, pp. 1055–1064, 1985
- [29] M. Bergman, "Stress intensity factors for circumferential surface cracks in pipes," Fatigue and Fracture Mechanics of Engineering Materials and Structure, vol. 18, no. 10, pp. 1155–1172, 1995.
- [30] A. Carpinteri, R. Brighenti, and A. Spagnoli, "Part-through cracks in pipes under cyclic bending," *Nuclear Engineering and Design*, vol. 185, no. 1, pp. 1–10, 1988.
- [31] A. Carpinteri and R. Brighenti, "Circumferential surface flaws in pipes under cyclic axial loading," *Engineering Fracture Mechanics*, vol. 60, no. 4, pp. 383–396, 1998.
- [32] A. Carpinteri, R. Brighenti, and A. Spagnoli, "Fatigue growth simulation of part-through flaws in thick-walled pipes under rotary bending," *International Journal of Fatigue*, vol. 22, no. 1, pp. 1–9, 2000.
- [33] I. Raju and J. Newman, Stress-Intensity Factors for Circumferential Surface Cracks in Pipes and Rods under Tension and Bending Loads, Fracture Mechanics, 17th ed. West Conshohocken: ASTM International, 1986.

Copyright © 2025 by the authors. This is an open access article distributed under the Creative Commons Attribution License which permits unrestricted use, distribution, and reproduction in any medium, provided the original work is properly cited ($\frac{\text{CC BY 4.0}}{\text{CC BY 4.0}}$).